iScience

CellPress
OPEN ACCESS

Article

Light-Triggered Electron Transfer between a Conjugated Polymer and Cytochrome C for Optical Modulation of Redox Signaling

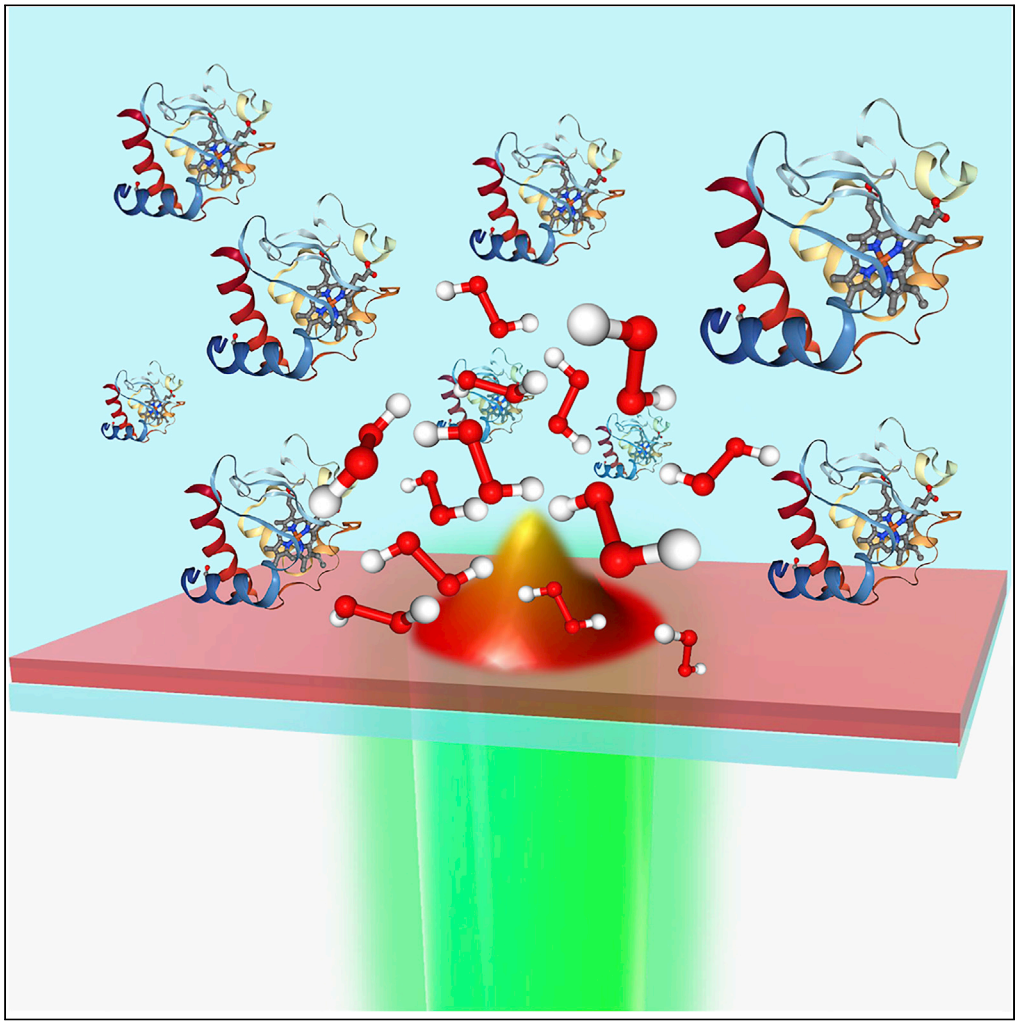

Ilaria Abdel Aziz, Marco Malferrari, Francesco Roggiani, Gabriele Tullii, Stefania Rapino, Maria Rosa Antognazza

stefania.rapino3@unibo.it (S.R.)
mariarosa.antognazza@iit.it (M.R.A.)

HIGHLIGHTS

Conjugated polymers and light modulate the redox state of cytochrome *c* protein

Phototransduction processes are clarified by electrochemical microscopy

The approach opens the way to selective optical triggering of protein redox state

Abdel Aziz et al., iScience *23*, 101091
May 22, 2020
https://doi.org/10.1016/j.isci.2020.101091

iScience

CellPress
OPEN ACCESS

Article

Light-Triggered Electron Transfer between a Conjugated Polymer and Cytochrome C for Optical Modulation of Redox Signaling

Ilaria Abdel Aziz,[1,2,4] Marco Malferrari,[3,4] Francesco Roggiani,[3] Gabriele Tullii,[1,2] Stefania Rapino,[3,*] and Maria Rosa Antognazza[1,5,*]

SUMMARY

Protein reduction/oxidation processes trigger and finely regulate a myriad of physiological and pathological cellular functions. Many biochemical and biophysical stimuli have been recently explored to precisely and effectively modulate intracellular redox signaling, due to the considerable therapeutic potential. Here, we propose a first step toward an approach based on visible light excitation of a thiophene-based semiconducting polymer (P3HT), demonstrating the realization of a hybrid interface with the Cytochrome *c* protein (CytC), in an extracellular environment. By means of scanning electrochemical microscopy and spectro-electrochemistry measurements, we demonstrate that, upon optical stimulation, a functional interaction between P3HT and CytC is established. Polymer optical excitation locally triggers photoelectrochemical reactions, leading to modulation of CytC redox activity, either through an intermediate step, involving reactive oxygen species formation, or via a direct photoreduction process. Both processes are triggered by light, thus allowing excellent spatiotemporal resolution, paving the way to precise modulation of protein redox signaling.

INTRODUCTION

Precise and selective modulation of biochemical reactions in living systems has been harvesting more and more interest in the latest years, due to its enormous therapeutic potential. Intracellular reduction-oxidation reactions trigger important physiological and pathological processes, being at the base both of cell metabolism, differentiation and proliferation, and of vital functions such as cellular respiration, homeostasis, and excitability (Forrester et al., 2018; Zhu and Thompson, 2019).

Several chemical tools have been successfully developed to target different sub-cellular organelles and redox-based specific functions, leading to unprecedented understanding and effective modulation of metabolism (Song et al., 2017). Unfortunately, the biochemical approach presents several drawbacks, being irreversible and time consuming, scarcely tunable and with limited spatiotemporal resolution. Physical stimuli, including ultrasound, heat, and electrical and magnetic stimulations, have been proposed as a valuable alternative to overcome these limitations (Deforest and Tirrell, 2015; Jiang and Pu, 2018; Wang and Lei, 2018; Huang et al., 2019; Lyu et al., 2019).

Modulation of redox signaling by light excitation is one of the most promising strategies, offering unrivalled resolution both in space and time, full reversibility, high versatility, and minimal invasiveness (Park et al., 2015; Kang et al., 2018; Li et al., 2019). The lack of natural absorbers, however, implies the need for developing suitable tools for efficient and reliable phototransduction. As recently reviewed in (Antognazza et al., 2019), two different approaches have been developed so far, based either on optogenetic tools, or on the use of exogenous, photocatalytic materials. The second possibility, although usually providing limited selectivity, allows for avoiding viral transfer and for working at light power density lower or comparable to those required by optogenetics. Moreover, exogenous stimulation can rely on a wide library of both inorganic and organic materials, in the form of micro- and nano-shaped devices (Tian and Lieber, 2013; Genchi et al., 2017a, 2017b; Tian et al., 2018; Jiang and Tian, 2018; Jiang et al., 2018). Even though inorganic materials offer higher photoelectrochemical activity and stability with respect to organic ones, their poor long-term biocompatibility strongly limited their applicability *in vivo* so far (Genchi et al.,

[1]Center for Nano Science and Technology@PoliMi, Istituto Italiano di Tecnologia, via Pascoli 70/3, 20133 Milano, Italy

[2]Politecnico di Milano, Dipartimento di Fisica, Piazza L. Da Vinci 32, 20133 Milano, Italy

[3]Università di Bologna, Dipartimento di Chimica "Giacomo Ciamician", via Francesco Selmi 2, 40126 Bologna, Italy

[4]These authors contributed equally

[5]Lead Contact

*Correspondence: stefania.rapino3@unibo.it (S.R.), mariarosa.antognazza@iit.it (M.R.A.)

https://doi.org/10.1016/j.isci.2020.101091

2017a, 2017b). Contrariwise, organic compounds offer a reliable, biocompatible alternative, supported by flexible fabrication methods and easy tuning of the optical and electrochemical properties. Conjugated polymers have found a central role in a wide variety of biotechnological applications thanks to their superior biocompatibility and long-term stability in a biological environment (Maya-Vetencourt et al., 2017). Mixed ionic/electronic conductivity typical of conducting polymers, coupled to good electrochemical stability, has been exploited for the realization of protein-functionalized electrodes (López-Bernabeu et al., 2017). In this context, the use of light as a physical stimulus may offer interesting paths, alternative to electrical stimulation, for selective and touchless modulation of the cell functions. It has been demonstrated that, upon photostimulation, thin films of a prototypical organic semiconductor, namely poly-3-hexyl-thiophene (P3HT), exhibit a stable and efficient photocatalytic activity in aqueous environment (Bellani et al., 2014, 2015; Mosconi et al., 2016; Rojas et al., 2016). Very recently, P3HT-based nanoparticles have been reported to efficiently modulate reactive oxygen species (ROS) production and intracellular Ca^{2+} trafficking (Tortiglione et al., 2017; Bossio et al., 2018; Moros et al., 2018). Semiconducting polymer nanoparticles, in particular, are emerging as highly promising tools in advanced biophotonics, not only for highly sensitive molecular imaging but also for touchless modulation of biological events, including protein ion channels physiology and physiopathology, enzymatic activity, and gene expression (Jiang and Pu, 2018; Lyu et al 2016, 2019). Potentially endless opportunities in polymer organic synthesis together with high versatility of organic devices fabrication technologies are paving the way to the next-generation of biophotonics therapeutic approaches. Few other organic nanobiocatalysts have been also reported for efficient photoactivation of intracellular redox signaling, including other organic semiconducting polymers (Lyu et al., 2016, 2018; Wang et al., 2018) and carbon-based nanomaterials (Chen et al., 2019; Guo et al., 2017; Liu et al., 2016). However, the functional interaction among visible light, semiconducting polymers, and protein redox activity has been considered to a very limited extent, so far, as a possible choice for cell metabolism control (Li and Pu, 2019). The successful implementation of this approach cannot overlook the detailed understanding and characterization of the photochemical and photophysical processes occurring at the hybrid interface between the light-sensitive organic material and the physiologically relevant intracellular targets, first in a simpler, extracellular environment and successively in the cell cytosol. Efforts are being directed toward the quantification of photogenerated moieties in water environment, as reactive oxygen species (Gryszel et al., 2019), the research being still at a very embryonal stage.

In this work, we focus on the functional interaction between regio-regular P3HT and a protein of pivotal importance in the respiratory chain, Cytochrome *c* (CytC). The latter is located in intramembrane space of mitochondria, and it can associate with integral membrane proteins across the inner membrane of mitochondria. CytC has a crucial role in the final reactions of oxidative phosphorylation, which leads to the ATP synthesis, being responsible for the transfer of one electron from complex III to complex IV through its heme C group (Ow et al., 2008; Yeagle, 2011). Several mitochondrial diseases are directly linked to alterations in physiological functions of the transmembrane respiratory complexes (Gorman et al., 2016), among which pathologies as tubulopathy, encephalopathy, and liver failure are associated to complex III deficiency (De Lonlay et al., 2001). Therefore, the possibility of introducing on-demand electron transfer actuators in the respiratory chain is raising more and more interest as possible therapeutic treatment.

Here, we successfully couple the photocatalytic activity of P3HT thin films with the redox properties of CytC, in an extracellular environment. Scanning electrochemical microscopy (SECM) offers the unique opportunity to characterize the reactivity at the interface with a high spatial and temporal resolution (Lin et al., 2018; Malferrari et al., 2019a, 2019b, Rapino et al., 2014, 2015; Soldà et al., 2017), giving an insight on the local electrochemical processes promoted by the light at the interface. By means of SECM and spectro-electrochemistry, we demonstrate that polymer photoexcitation deterministically leads to CytC reduction. Furthermore, we provide evidences of the occurrence of direct electron transfer reactions at the polymer/CytC interface.

Besides, a mitochondria-targeting strategy still needs to be developed; the capability to finely, optically tune the CytC activity may open interesting perspectives in the study of mitochondria pathophysiological conditions, providing a versatile, minimally invasive, and highly localized tool to modulate the intracellular redox state.

RESULTS AND DISCUSSION

Photocurrent Generation in Hybrid P3HT/Electrolyte:CytC Interfaces

Recent literature showed that P3HT thin films exposed to saline solutions (KRH and NaCl) fully preserve the capability to generate photocurrent upon visible light excitation (Fumagalli et al., 2015). In this work, we adopt highly controllable experimental conditions, by exposing P3HT thin films deposited on top of ITO conductive substrates (ITO/P3HT) to a neutral phosphate buffer solution (PB, 4 mM, pH 7.4). The photocurrent action spectrum, measured in a two-electrode configuration and at the open circuit potential (V_{oc}, 0.17 V versus Ag/AgCl), does not show relevant differences as compared with the P3HT photocurrent spectrum in solid phase or in other hybrid solid/liquid devices (Antognazza et al., 2009). We observe a symbatic behavior, with maximum current density at 550 nm and two shoulders at 470 nm and 600 nm (Figure S1, red dotted line). The origin of the current signal has been unambiguously identified with photofaradaic reactions occurring at the polymer surface, in particular oxygen reduction processes (Bellani et al., 2015). Briefly, upon photoexcitation, polaron states are generated on ultrafast timescales within the polymer bulk. Noteworthy, penetration of water within the polymer bulk has been reported to considerably increase the surface area and to establish a volumetric interfacial capacitance (Tullii et al., 2017). Excited states can dissociate into free charges, electrons, and holes, at the diffused electrolyte and ITO interfaces, respectively. Previous reports show that the ITO contact acts as a holes sink, whereas electrons give rise to oxygen reduction processes in the liquid phase, thus sustaining a photocurrent of faradaic origin. The metastable superoxide radical anion O_2^- is then expected to undergo a rapid dismutation process ($k = 5 \times 10^5\ M^{-1}s^{-1}$, according to (Ohara and Sayuri, 2012)) leading to formation of hydrogen peroxide (H_2O_2). A quantitative evaluation of the process efficiency and its spatial extension is of a paramount importance for any possible perspective application in the optical modulation of the intracellular activity. To face this challenge, we employ SECM technique, focusing our attention on H_2O_2 detection upon polymer photoexcitation (Figure 1). It has been widely demonstrated that nanoporous black platinum (BP)-modified electrodes can selectively detect H_2O_2 with high sensitivity (Amatore et al., 2008; Lin et al., 2018; Malferrari et al., 2019a, 2019b). In this work, BP ultramicroelectrodes were employed as SECM probe to locally sense photoinduced H_2O_2 production at the ITO/P3HT/electrolyte interface (see Figure 1A for a schematic representation and Transparent Methods section for details of the experimental setup). The SECM probe was positioned at a distance of about 25 μm from the substrate by performing approach curves (see Transparent Methods). Once positioned, scan lines were carried out at constant height along the x-direction on the illuminated area of the sample (Figure 1A). P3HT is photoexcited by the filtered emission of a mercury lamp, focused on the sample through a microscope objective. Figure 1B (lower panel) shows the oxidation current recorded at the BP microelectrode as a function of the linear displacement along the x-direction of the scanning working electrode. The current intensity profile is in agreement with the Gaussian profile of the excitation beam (upper panel). The current signal is due to the oxidation of H_2O_2 at the BP electrode, the signal being proportional to the amount of H_2O_2 generated at the polymer/electrolyte interface upon photostimulation. Control measurements on polymer in dark condition and on ITO upon illumination (blue and black curves, respectively) do not show significant H_2O_2 generation, as no oxidation current is recorded at the probe electrode, as expected. Therefore, the generation of H_2O_2 is spatially localized within the illuminated area of P3HT thin film (red curve). The temporal evolution of H_2O_2 production upon photostimulation at a distance of 20–25 μm from the substrate (illumination duration, 100 s) is also monitored by chronoamperometry (Figure 1C). The fast-current transient recorded at the beginning of the trace is due to the charging of the double layer. The current signal associated to H_2O_2 production by photoexcited P3HT (red curve) shows a 2.5 higher signal as compared with control, thus indicating substantial H_2O_2 production. Based on the measured values and photoexcitation spot size, we estimate a local concentration of produced hydrogen peroxide of ~700 nM within a volume of about $7 \times 10^6 \mu m^3$. The ITO and bare glass control samples (black and gray curves, respectively) display, upon photoexcitation, a current signal in the order of tens of pA, which can be ascribed to photocurrent promoted at the nanoporous BP electrode by light illumination.

Having assessed the capability of photostimulated ITO/P3HT substrate to promote H_2O_2 production, we turn our attention to investigating the interaction with the CytC protein. The addition of oxidized CytC (10 μM) to the PB solution does not detectably modify the steady-state photocurrent action spectrum, measured in a two-electrode configuration, typical of the ITO/P3HT/PB device architecture (Figure S1, green dotted line). Importantly, SECM chronoamperometry measurements display a markedly different behavior in the first few seconds (<10 s) after light onset (Figures 1D and S2). An additional current signal component is observed in presence of CytC further evidenced by data fitting (Figure S3). Although the

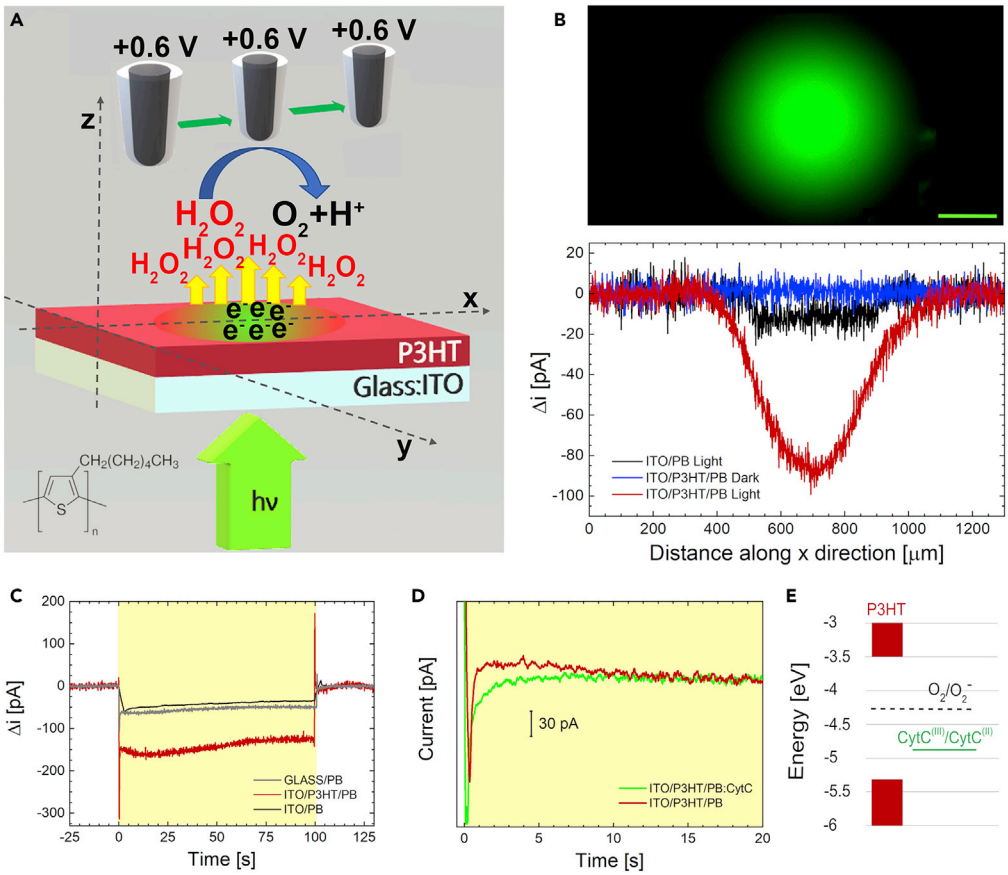

Figure 1. Hybrid P3HT/PB:CytC Interface Locally Generates H_2O_2 upon Visible Light

(A) Schematic representation of the detection strategy of H_2O_2 production upon P3HT polymer photoexcitation. The chemical structure of P3HT is reported.

(B) Upper panel: fluorescence image of the illuminated region of the sample. Lower panel: SECM scan lines of H_2O_2 production measured as H_2O_2 oxidation current at the black platinum probe. P3HT in the dark (blue), P3HT under illumination (red), ITO under illumination (black). Scale bar: 200 μm.

(C) Oxidation current recorded at the black platinum microelectrode positioned in the proximity of the substrate: P3HT (red), ITO (black) and optical glass (gray). Time zero corresponds to the illumination onset. Optical stimulus duration, 100 s.

(D) Time course of H_2O_2 production upon polymer photoexcitation, in 4 mM phosphate buffer (red trace) or in buffer enriched with 10 μM CytC (green trace). See Figure S2 (Transparent Methods) for details on trace representation.

(E) Energy diagram comparing P3HT Highest Occupied Molecular Orbital (HOMO) and Lowest Unoccupied Molecular Orbital (LUMO) (red shaded bars), CytC reduction (green line, see also Figure S4), and O_2/O_2^- reduction potential (dotted line, from (Krumova and Cosa, 2016)).

behavior of the ITO/P3HT/PB interface is reproduced by a single exponential decay, the addition of CytC to the PB implies the need for considering a double exponential fitting curve (Table 1). These features may indicate an active involvement of CytC protein in the photoelectrochemical processes occurring at the P3HT/PB interface. This hypothesis is in agreement with the P3HT and CytC relative energy diagram, reported in Figure 1E. The CytC reduction potential was calculated from cyclic voltammetry measurements (Figure S4) and are in agreement with those reported by (Gong et al., 2017), suggesting that the electron transfer processes between the two moieties are energetically favored. Importantly, the oxygen reduction potential level (Krumova and Cosa, 2016) falls within the P3HT band gap and above CytC reduction potential.

To elucidate the role of CytC in the photocatalytic H_2O_2 production process by P3HT substrates, SECM approach curves to ITO/P3HT and ITO substrates were carried out in presence and absence of 10 μM CytC in solution. SECM approach curves are a valuable approach to characterize reduction/oxidation

Condition	Fitting Equation	Time Constants
ITO/P3HT/PB	$y = A_1*\exp(-x/t_1) + y_0$	t_1 = (0.157 ± 0.002) s
ITO/P3HT/PB:CytC	$y = A_1*\exp(-x/t_1) + A_2*\exp(-x/t_2) + y_0$	t_1 = (0.108 ± 0.003) s t_2 = (1.160 ± 0.020) s

Table 1. The Presence of CytC Affects Photocurrent Dynamics

Fitting time constants for recorded current signals. The current signals associated to ITO/P3HT/PB and ITO/P3HT/PB:CytC are best fitted by a single and double exponential equation, respectively. Decay time constants are reported as mean ± SD.

processes occurring at liquid/liquid and liquid/solid interfaces (Wittstock et al., 2007; Lin et al., 2018). Figure 2 shows approach curves obtained in dark condition or upon photostimulation on ITO/P3HT or ITO substrates. The BP microelectrode was biased at 0.6 V versus Ag/AgCl (KCl 3 M) in order to carry out generator (ITO/P3HT substrate) – collector (BP microelectrode) approach curves. The recorded faradaic current is supposed to increase with increasing proximity to the substrate upon production of the detected species, namely H_2O_2. At the same time, the hindering diffusion effect due to the presence of the substrate is expected to decrease the recorded current as the substrate-tip distance becomes closer.

The approach current associated to bare ITO in absence and presence of CytC (panels A and C, respectively), in dark or upon photostimulation, is compared with the signal recorded for P3HT in similar conditions (panels B and D, respectively). Neither the illumination protocol nor the protein presence leads to detectable differences in the approach curves of bare ITO. Contrariwise, the presence of both the protein and light changes the approach dynamic for P3HT substrate (green dots curve in panel D). In fact, the collector current increases upon P3HT illumination in presence of CytC. H_2O_2 is detected at the BP tip up to 250 μm from the substrate. These results confirm that H_2O_2 production in the proximity of the substrate is fostered by the presence of CytC, suggesting a synergistic mechanism between P3HT and CytC in the oxygen reduction process and clearly indicating a close interaction between the two moieties. In absence of H_2O_2 collection, the approach results in a negative feedback curve, as expected in presence of the pure diffusion hindering effect (all curves of panels A, B, and C and gray curve of panel D).

We notice that chronoamperometry measurements carried out in the macroscopic environment of a standard three-electrode photoelectrochemical cell do not show a markedly different behavior in presence or absence of CytC in the buffer. Indeed, because of the lack of spatial resolution of this technique with respect to SECM, the aforementioned phenomenon cannot be observed in the macroscopic experimental conditions (Figure S5). Importantly, we stress out that in SECM measurements the P3HT thin film is neither biased nor grounded. This is a key feature toward future application of the technique for intracellular regulation of redox state, further confirming that the complex interplay between polymer photoexcitation, leading to photoelectrochemical processes, and CytC protein, is spatially confined at the hybrid solid/liquid interface and happens without the need of any wiring.

P3HT Photoexcitation Prompts CytC Reduction

The observed functional interaction between CytC protein and P3HT polymer is directly confirmed by spectroelectrochemical measurements (Figure 3). In order to simultaneously monitor the photocurrent generation in the P3HT-based photoelectrochemical cell and the oxidative state of the protein dissolved in the PB, we coupled polymer optical excitation with both chronoamperometry detection and optical absorption measurement in one single, home-made set-up (Figure S6).

The oxidation state of CytC can be easily detected by measuring its absorption spectrum in the spectral range between 520 and 560 nm (Figure 3A). The protein in the reduced state (dark green trace) shows two clearly distinct peaks at 520 nm and 550 nm, whereas the fully oxidized state (light green trace) is characterized by a broader, less resolved spectrum (Butt and Keilin, 1962). The optical absorption spectrum of P3HT thin film (red trace) and the emission spectrum of the light source used for polymer optical excitation (blue shaded area) are also shown. We notice that the optical excitation matches the conjugated polymer absorption and minimally overlaps with the one of CytC in either forms, thus allowing excluding concomitant optical excitation of the protein. Moreover, in order to avoid any scattering and reflection effect, LED source incidence direction is set at 90° with respect to the spectrophotometer optical path, and the

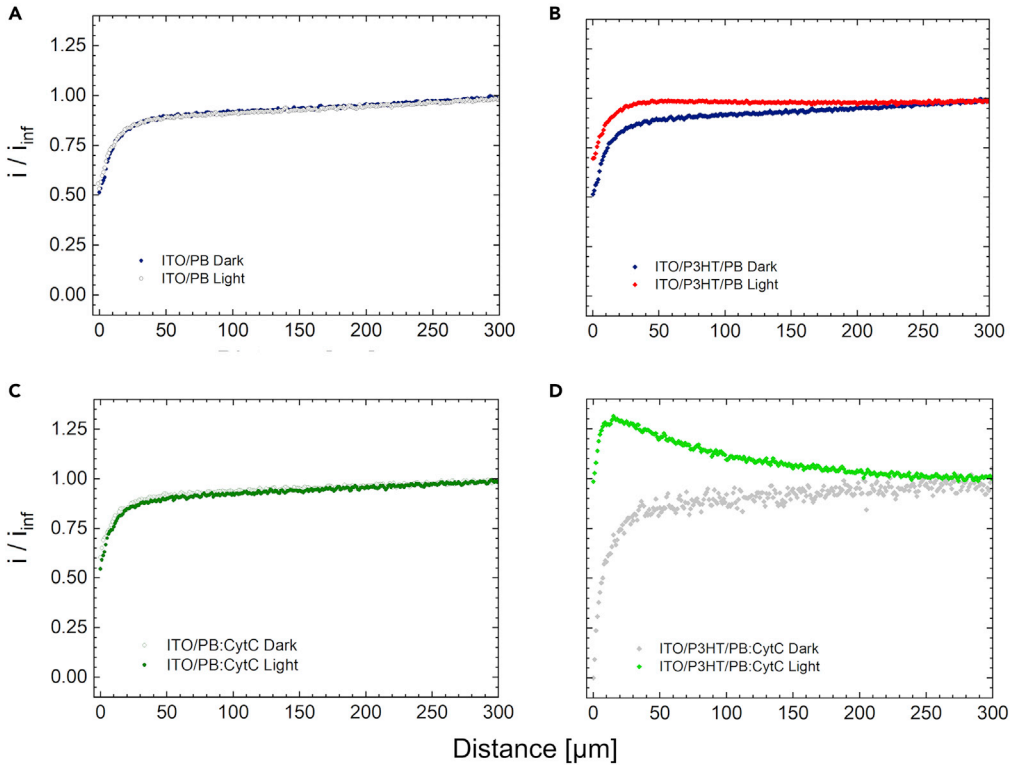

Figure 2. SECM Approach Curves to ITO and ITO/P3HT Substrates

Approach curves to ITO (A and C) and P3HT substrates (B and D) in absence or presence of 10 μM CytC (top and bottom panels, respectively), upon illumination or in dark conditions.

transmitted beam is properly screened. Spectrophotometer optical beam, probing CytC absorption, passes through the PB solution without any overlap with the P3HT thin film sample (Figure S6). Figure 3B shows the variation of the optical absorption spectra of CytC at increasing temporal duration of the P3HT photoexcitation protocol, from 0 (black solid line) up to 20 min (light green solid line). In these measurements, a negative bias of 200 mV with respect to open circuit condition was applied, to maximize the current generated by the polymer, in agreement with its photocathodic behavior in contact with the PB (see Figure S5 for chronoamperometry curves at different applied voltages, both in the presence and in absence of CytC, and related comments).

Upon continuous optical excitation of the polymer for 3 min (dark green solid line), the CytC absorption spectrum does not show any relevant change with respect to the reference condition in dark (black solid line). However, longer P3HT photoexcitation protocols (CW excitation up to 20 min, green traces) lead to a sizable variation of the CytC absorption spectrum, which visibly shifts from the oxidized to the reduced state. The typical absorption features of the latter show an enhancement in the optical absorbance of 5% and 16%, at 520 nm and 550 nm, respectively. This effect is already saturated upon a P3HT photoexcitation protocol lasting for 10 min. Absorption data clearly indicate a direct correlation between photoelectrochemical processes occurring at the P3HT/PB interface and the redox activity typical of the CytC protein. The dependence of the CytC absorption variation on application of external bias to P3HT further corroborates this result (Figure 3C). The ITO/P3HT/PB hybrid interface displays a photocathodic behavior. In particular, the current is significantly increased upon bias more negative than the open circuit potential (V_{oc}) value, whereas it is not affected by external bias more positive than the V_{oc} (Figure S5). Accordingly, no significant variation in the protein oxidation state is detected upon positive bias (red and light-red solid lines), being the signal intensity comparable with the non-illuminated control sample (gray solid line). Conversely, at the V_{oc} value, the 550 nm and 520 nm spectral features, typical of the CytC reduced state, are clearly visible (black solid line), and they are even more significantly enhanced upon negative bias (i.e., in the situation maximizing the polymer photocathodic current, Figure S5). A substantial difference is achieved upon application of −100 mV with respect to the V_{oc} (dark blue line), with the 550 nm peak

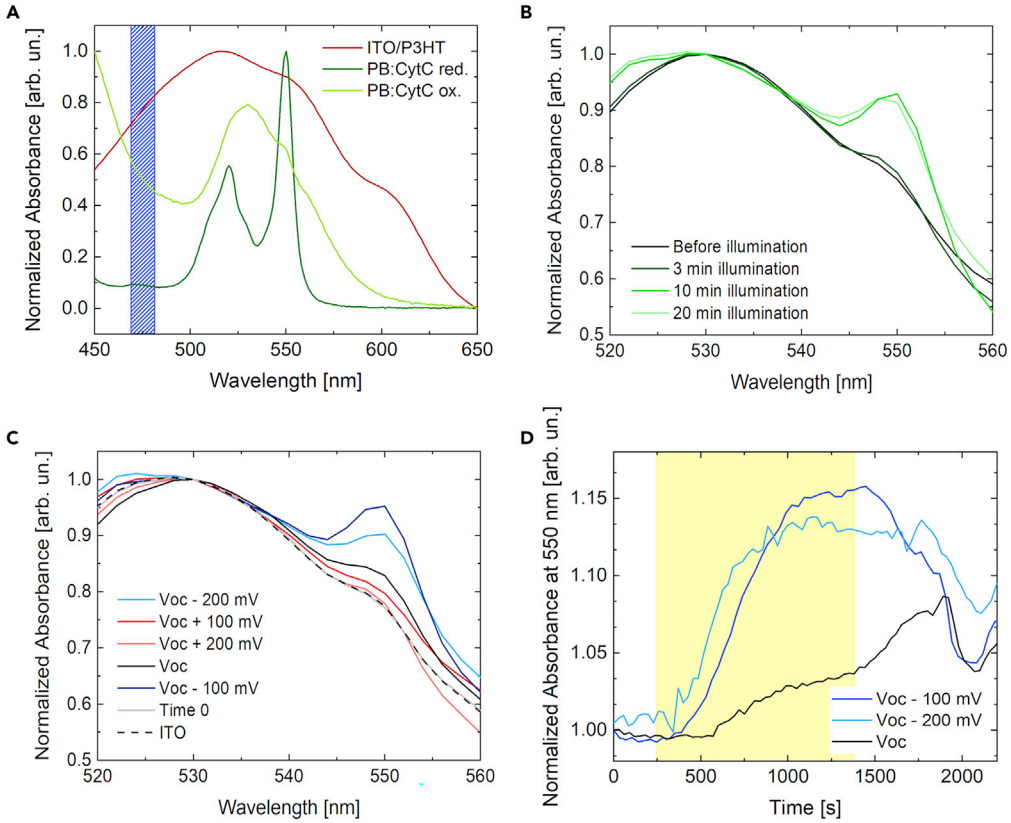

Figure 3. P3HT Photoexcitation Reduces CytC

(A) Absorbance spectra of oxidized and reduced CytC (light and dark green lines, respectively) and of P3HT solid film (red line). Polymer excitation is also represented by the blue-shaded rectangle.

(B) Absorbance variation of CytC before and after polymer CW photoexcitation for 3, 10, and 20 min. An external bias of −200 mV with respect to V_{OC} value is applied (see also Figure S6 for the sketch of the setup).

(C) Absorption variation of CytC before (time 0) and after P3HT CW photostimulation (20 min), as a function of the external bias. V_{OC}, ± 100 mV and ±200 mV potential values are applied during polymer excitation (see also Figure S5). The control measurement on a bare ITO electrode at −200 mV respect to V_{OC} is also reported, as a reference for direct photoreduction of CytC (dashed trace).

(D) Time variation of 550 nm absorption peak of CytC upon P3HT photoexcitation at V_{OC} (black solid line), V_{OC}– 100 mV (blue solid line), and V_{OC}– 200 mV (cyan solid line). See also Figure S7 for positive applied biases.

increasing by 17%. In the case of external bias equal to −200 mV with respect to V_{oc}, the relative variation of the 550 nm absorbance peak is 12% (light blue line). Based on the bias (Figure 3C) and temporal (Figure 3B) dependence, the link between CytC reduction processes and P3HT photostimulation clearly emerges. Reduction dynamics are better evidenced in Figure 3D, reporting the variation of the 550 nm peak over time upon negative applied bias. During illumination upon negative bias, temporal dynamics show three common regimes: (1) an initial phase, immediately after the light onset, in which no variation is recorded with respect to dark condition; (2) an intermediate phase, showing an increase of the relative weight of the feature at 550 nm on the overall absorption spectrum; (3) an equilibrium situation, in which no further changes in the spectrum are recorded. The temporal window corresponding to each phase clearly depends on the external bias. The recorded variation in the optical absorbance, as normalized with respect to the initial condition in dark, is 5% and 15%, for V_{OC} and V_{OC}– 200 mV versus Ag/AgCl external bias, respectively. We define the "response time" as the time required to observe an absorbance increase equal to 10% of the whole dynamic. The more negative the applied bias, the faster the response time, amounting to 429 ± 20.5 s and 276.5 ± 7.1 s for V_{OC} and V_{OC}– 200 mV, respectively. The negative applied bias fosters the electron migration toward the interface (Figure S5), leading to a sizable absorption change at earlier times, reflecting a higher CytC reduction rate. The dependence of both the absorbance variation and the response time on the applied bias highlights the role of the polymer mediated light stimulation.

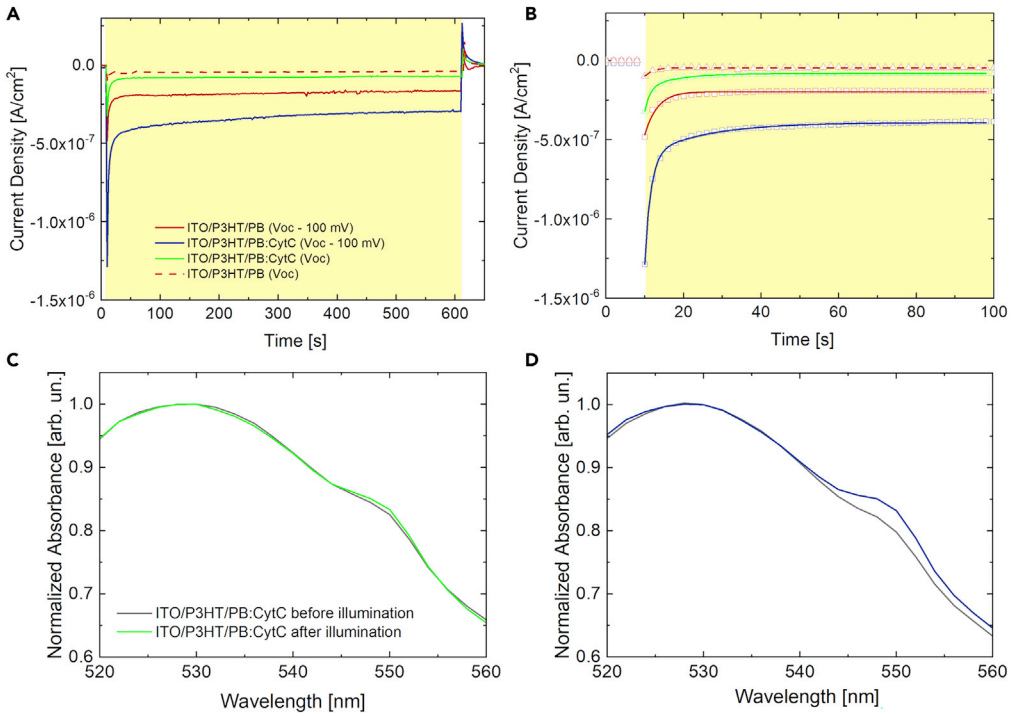

Figure 4. Molecular Oxygen Acts as Redox Mediator in the Photoexcited P3HT/PB:CytC Electron Transfer

(A) Chronoamperometry measurements in absence of oxygen (see Figure S8 for LSV measurements) on ITO/P3HT/PB and ITO/P3HT/PB:CytC at V_{OC} versus Ag/AgCl (red dashed and green solid traces, respectively) and on ITO/P3HT/PB and ITO/P3HT/PB:CytC at V_{OC} -100 mV versus Ag/AgCl (red and blue solid traces, respectively).

(B) Chronoamperometry decay dynamics fitting (see Table 2 for details).

(C) Absorbance of CytC before (black solid line) and after (green solid line) P3HT photostimulation, in V_{OC} condition.

(D) Absorbance of CytC before (black solid line) and after (blue solid line) P3HT photostimulation, upon external negative bias (V_{OC}– 100 mV versus Ag/AgCl).

It is worth noting that CytC absorption spectrum minimally overlaps with LED light source used for photoexcitation (Figure 3A). In order to exclude any possible contribution from direct photoexcitation of CytC, we carried out spectroelectrochemical measurements using bare ITO electrode, reported in Figure S7. Upon visible light excitation the CytC solution does not show relevant absorbance changes, thus ruling out direct photoreduction processes. Furthermore, CytC reduction potential against P3HT and ITO electrodes is lower than the applied negative bias by 0.155 $\pm$ 0.015 V versus Ag/AgCl (see CytC cyclic voltammetry with P3HT and ITO working electrode, Figure S4). Thus, we can safely exclude any possible contribution to the observed variation in the absorption spectra both from direct CytC photoreduction (i.e., not mediated by the polymer photocurrent generation) and from direct CytC reduction processes upon external bias. Accordingly, control measurements carried out onto the ITO/PB:CytC device allow to conclusively exclude both these two effects (Figure S7, black solid line) and further confirm that CytC reduction is unambiguously, directly linked to P3HT photocathodic current. Overall, data in Figure 3 demonstrate the occurrence of electron transfer processes between the organic semiconductor and the protein, triggered by polymer photostimulation.

Role of Molecular Oxygen in the Light-Driven P3HT/PB:CytC Electron Transfer

P3HT-based photoelectrochemical systems working in aqueous electrolytes were recently proposed as efficient oxygen reduction systems (Fumagalli et al., 2015). In particular, the role of molecular oxygen dissolved in the electrolyte was demonstrated to be the key component to sustain the photocathodic current generation (Bellani et al., 2014). Thus, considering the role of CytC in cellular respiration processes, it is interesting to investigate in detail the O_2 contribution also in the more complex P3HT/PB:CytC hybrid system.

Condition	Fitting Equation	Bias	Time Constant
ITO/P3HT/PB	$y = A_1*\exp(-x/t_1) + y_0$	V_{OC} versus Ag/AgCl	$t_1 = 2.51 \pm 0.33$ s
		V_{OC}– 100 mV versus Ag/AgCl	$t_1 = 3.20 \pm 0.001$ s
ITO/P3HT/PB:CytC	$y = A_1*\exp(-x/t_1) + A_2*\exp(-x/t_2) + y_0$	V_{OC} versus Ag/AgCl	$t_1 = 9.37 \pm 0.68$ s $t_2 = 1.042 \pm 0.22$ s
		V_{OC}– 100 mV versus Ag/AgCl	$t_1 = 15.38 \pm 0.007$ s $t_2 = 1.529 \pm 0.002$ s

Table 2. Molecular Oxygen Affects Photocurrent Dynamics

Fitting time constants for chronoamperometries carried out in controlled nitrogen atmosphere. As in the case of exposure to oxygen dissolved in the buffer, current signals recorded in ITO/P3HT/PB and ITO/P3HT/PB:CytC samples are fitted with a single and double exponential curve, respectively, both in open circuit condition and upon negative bias. Decay time constants are reported as mean ± SD.

We carry out electrochemical and spectro-electrochemical measurements in nitrogen-controlled atmosphere (Figure 4). Linear sweep voltammetry and chronoamperometry scans (Figures S8 and 4A, respectively) show that, upon a decrease up to 80% of dissolved oxygen in the PB bath, the current density is also considerably reduced, by more than one order of magnitude, both in absence and in presence of CytC. Interestingly, the faradaic component of the photocurrent of P3HT in CytC solution upon dissolved O_2 removal is sensibly higher (by a factor of 81%, as evaluated at 400 s after photoexcitation onset) than the one recorded in bare PB. This may indicate a direct transfer of electrons from the photoexcited polymer to the protein. This effect is more pronounced with the application of V_{oc}– 100 mV versus Ag/AgCl bias (red and blue solid lines in Figure 4A), possibly denoting a higher affinity between P3HT and CytC for energy transfer. The oxygen removal from the buffer solution dramatically decreases the oxygen-dependent photoelectrochemical processes, highlighting the presence of a direct electron transfer between the photoexcited polymer and the protein. In order to evaluate the time constants of both these processes, we carried out an exponential fit of the chronoamperometry signals. Interestingly, chronoamperometry curves recorded on ITO/P3HT/PB samples were fitted by a single-exponential curve. Conversely, ITO/P3HT/PB:CytC data are fitted by a double-exponential curve (Figure 4B).

This observation may further suggest the occurrence of a secondary photoelectrochemical process, involving not only direct interaction between photoexcited P3HT polymer and remaining oxygen in the PB bath but also direct interaction between P3HT polymer and CytC, even in nitrogen-controlled atmosphere. Extracted time constants are reported in Table 2.

We observe that the time constant associated to the oxygen reduction photoelectrochemical process (t_1) is similar both in presence and in absence of CytC, in the order of few s, and in both cases the rate is faster upon negative bias ($k_1 = 0.416 \pm 0.12\ s^{-1}$ versus $k_{1bias} = 0.312 \pm 0.0013\ s^{-1}$). Conversely, the rate of the second decay component, attributed to P3HT/CytC direct electron transfer process, is sizably faster, at V_{oc} ($k_2 = 0.11 \pm 0.015\ s^{-1}$) and even more upon negative bias ($k_{2bias} = 0.065 \pm 0.0006\ s^{-1}$).

Finally, we validated the occurrence of a direct interaction between P3HT polymer and CytC, by means of spectroelectrochemical measurements in nitrogen-controlled atmosphere (Figures 4C and 4D). Figure 4C reports the absorption spectrum of CytC in partially degassed V_{oc} condition, before and after P3HT photoexcitation (10 min, black and green lines, respectively). In nitrogen-controlled atmosphere, no sizable difference between the pre- and after illumination spectra is observed. However, when the working P3HT electrode is held at V_{oc}– 100 mV versus Ag/AgCl bias (Figure 4D), a 1% increase in the absorption spectrum of CytC at 550 nm is detected, thus confirming that the protein undergoes a reduction process as a direct consequence of polymer photoexcitation, even in almost complete absence of dissolved oxygen in the electrolyte solution. In summary, the combination of scanning electrochemical microscopy and spectro-photoelectrochemical experimental data allows elucidating the complex interplay among polymer photocatalytic behavior, CytC redox processes, and oxygen dissolved in water. Overall, the occurrence of three different surface processes, partially overlapped, is evidenced (Figure 5).

As mentioned before, upon photoexcitation, polaron states are created on ultrafast timescales within the polymer bulk, which subsequently dissociate into free charges. The photocurrent relative sign is

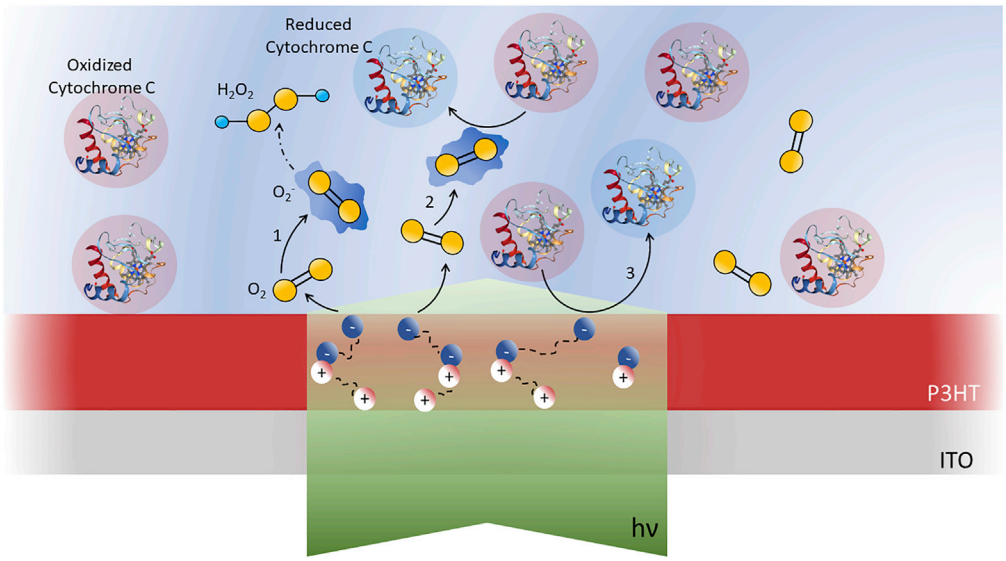

Figure 5. Photocatalysis of P3HT Actively Regulates CytC Redox State Both through Direct- and Oxygen-Mediated Electron Transfer

Sketch of polymer-mediated, light-triggered electrochemical reactions occurring at the hybrid solid-liquid interface between rr-P3HT, CytC, and PB electrolyte solution. Light (green shaded area) impinges on the polymer thin film from bottom ITO side and generates polaron states, which undergo fast dissociation processes into free charges. Electrons predominantly migrate toward electrolyte interface and allow electron transfer reactions. Three photoelectrochemical reactions are observed: (1) interaction with oxygen dissolved in the aqueous electrolyte (yellow), superoxide formation, and subsequent hydrogen peroxide formation; (2) superoxide formation and subsequent CytC reduction (represented as red-blue transition of the CytC protein); (3) direct interaction between P3HT charged states and CytC(III).

compatible with electron migration toward the electrolyte interface and efficient electron transfer sustaining superoxide formation. The latter can give rise to formation of both reactive oxygen species, finally ending with H_2O_2 formation (Equation 1), and CytC reduction (Equation 2). Interestingly, a direct interaction between photoexcited polymer charged states and CytC is also observed, leading to a parallel, alternative path for CytC reduction (Equation 3).

$$O_2 + e^- \rightarrow O_2^-$$

$$O_2^- + e^- + 2H^+ \rightarrow H_2O_2 \quad \text{(Equation 1)}$$

$$O_2^- + CytC^{(III)} \rightarrow CytC^{(II)} + O_2 \quad \text{(Equation 2)}$$

$$P3HT^- + CytC^{(III)} \rightarrow CytC^{(II)} + P3HT \quad \text{(Equation 3)}$$

Polymer/CytC direct, light triggered interplay is strongly spatially localized at the polymer surface, and it can be identified by the use of spatially resolved experimental techniques. Alternatively, it can be partially disentangled from concomitant photoactivated reactions by reducing the concentration of dissolved oxygen and by proper fitting of chronoamperometry dynamics.

Conclusions

In summary, we report on a functional, hybrid interface composed of a prototypical conjugated polymer, based on a thiophene derivative, and CytC protein. Upon photoexcitation, the polymer thin film behaves as intrinsic photocatalyst through oxygen reduction. Scanning electrochemical measurements carried out upon polymer photoexcitation allowed to precisely quantify the efficiency of the process, ending with H_2O_2 formation, and to provide an estimation of its spatial extension.

Interestingly, polymer photoexcitation and subsequent light-triggered electron transfer reactions lead to two modulation mechanisms of the protein redox activity, as expected based on polymer/protein electrochemical affinity. The first phototransduction process involves an intermediate step, sustained by superoxide formation. The second one is based on a direct electron transfer between the organic semiconductor and the protein, which leads to CytC reduction reaction, more evident at reduced concentration of dissolved oxygen. Both processes are triggered by light, thus in principle allowing redox signaling

modulation with excellent spatial and temporal resolution, as compared with biochemical modulation tools. Importantly, we notice that in SECM measurements the P3HT photoactuator is completely floating, indicating that the aforementioned processes do occur in open circuit conditions, thus not requiring any wiring.

In perspective, our approach may be usefully applied to spatio-temporally confined modulation of intracellular redox signaling, promoting the development of specific targeting strategies that are still lacking. The use of biocompatible conjugated polymers endowed with photocatalytic properties potentially offers the unprecedented opportunity of chemical functionalization with specific drugs and selective targeting of subcellular organelles, paving the way to precise, on-demand cell metabolism modulation, in a reversible manner and by using a completely gene-less, contactless approach.

Limitations of the Study

We reported on a highly localized, light-driven electron transfer process between a protein and a semiconducting polymer electrode. The combined use of optical excitation and exogenous photoactuators is a promising approach for highly selective and spatially controlled modulation of the cellular redox state, at the organelles level. However, in the current work we employ, as a proof of concept, a planar, thin film electrode. The potential of the reported approach should be demonstrated by engineering biocompatible, P3HT-based beads, safely and selectively targeted to mitochondria. Further steps will assess the photoelectrochemical efficiency within the cell cytosol as well as the long-term dose-response for metabolism modulation in both physiological and pathophysiological conditions.

Resource Availability

Lead Contact

Further information and requests for resources and materials should be directed to and will be fulfilled by the Lead Contact, Dr. Maria Rosa Antognazza (mariarosa.antognazza@iit.it).

Materials Availability

This study did not generate new unique reagents.

Data and Code Availability

Source data for the figures published in this the paper will be available at: https://zenodo.org/communities/lionheartedhorizon2020/?page=1&size=20.

METHODS

All methods can be found in the accompanying Transparent Methods supplemental file.

SUPPLEMENTAL INFORMATION

Supplemental Information can be found online at https://doi.org/10.1016/j.isci.2020.101091.

ACKNOWLEDGMENTS

MRA acknowledges support by the European Research Council (ERC) under the European Union's Horizon 2020 research and innovation program "LINCE," grant agreement n. 803621. MRA and SR acknowledge support by the European Union's Horizon 2020 research and innovation program, H2020-FETOPEN-01-2018-2020 (FET-Open Challenging Current Thinking), "LION-HEARTED," grant agreement n. 828984.

AUTHOR CONTRIBUTIONS

IAA and MM contributed equally to this work. MRA and SR planned and organized the work. IAA carried out the electrochemical and spectro-electrochemical experiments, with help from GT. MM, FR, and SR carried out and interpreted SECM data. All authors contributed to data analysis and interpretation. IAA, SR, and MRA wrote the main manuscript, with contribution from all authors.

DECLARATION OF INTEREST

There are no conflicts to declare.

Received: December 18, 2019
Revised: March 2, 2020
Accepted: April 16, 2020
Published: May 22, 2020

REFERENCES

Amatore, C., Arbault, S., Guille, M., and Lemaître, F. (2008). Electrochemical monitoring of single cell secretion: vesicular exocytosis and oxidative stress. Chem. Rev. *108*, 2585–2621.

Antognazza, M.R., Ghezzi, D., Musitelli, D., Garbugli, M., and Lanzani, G. (2009). A hybrid solid-liquid polymer photodiode for the bioenvironment. Appl. Phys. Lett. *94*, 2–4.

Antognazza, M.R., Abdel Aziz, I., and Lodola, F. (2019). Use of exogenous and endogenous photomediators as efficient ROS modulation tools: results and perspectives for therapeutic purposes. Oxid. Med. Cell Longev. *2019*, 2867516.

Bellani, S., Fazzi, D., Bruno, P., Giussani, E., Canesi, E.V., Lanzani, G., Antognazza, M.R., Fisica, D., Chimica, D., Chimica, I., et al. (2014). Reversible P3HT/oxygen charge transfer complexidentification in thin films exposed to direct contact with water. J. Phys. Chem. C *118*, 6291–6299.

Bellani, S., Ghadirzadeh, A., Meda, L., Savoini, A., Tacca, A., Marra, G., Meira, R., Morgado, J., Di Fonzo, F., and Antognazza, M.R. (2015). Hybrid organic/inorganic nanostructures for highly sensitive photoelectrochemical detection of dissolved oxygen in aqueous media. Adv. Funct.Mater. *25*, 4531–4538.

Bossio, C., Aziz, I.A., Tullii, G., Zucchetti, E., Debellis, D., Zangoli, M., DiMaria, F., Lanzani, G., and Antognazza, M.R. (2018). Photocatalytic activity of polymer nanoparticles modulates intracellular calcium dynamics and reactive oxygen species in HEK-293 cells. Front. Bioeng.Biotechnol. *6*, 1–17.

Butt, W.D., and Keilin, D. (1962). Absorption spectra and some other properties of cytochrome c and of its compounds with ligands. Proc. R. Soc.Lond. B Biol. Sci. *156*, 429–458.

Chen, P., Ma, Y., Zheng, Z., Wu, C., Wang, Y., and Liang, G. (2019). Facile syntheses of conjugated polymers for photothermaltumour therapy. Nat. Commun. *10*, 1–10.

Deforest, C.A., and Tirrell, D.A. (2015). A photoreversible protein-patterning approach for guiding stem cell fate in three-dimensional gels. Nat. Mater. *14*, 523–531.

Forrester, S.J., Kikuchi, D.S., Hernandes, M.S., Xu, Q., and Griendling, K.K. (2018). Reactive oxygen species in metabolic and inflammatory signaling. Circ. Res. *122*, 877–902.

Fumagalli, F., Bellani, S., Schreier, M., Leonardi, S., Rojas, H., Ghadirzadeh, A., Tullii, G., Savoini, A., Marra, G., Meda, L., et al. (2015). Hybrid organic-inorganic H2-evolving photocathodes: understanding the route towards high performances organic photoelectrochemical water splitting. J. Mater. Chem. A, 2178–2187.

Genchi, G.G., Marino, A., Grillone, A., Pezzini, I., and Ciofani, G. (2017a). Remote control of cellular functions: the role of smart nanomaterials in the medicine of the future. Adv. Healthc. Mater. *6*, https://doi.org/10.1002/adhm.201700002.

Genchi, G.G., Marino, A., Tapeinos, C., and Ciofani, G. (2017b). Smart materials meet multifunctional biomedical devices: current and prospective implications for nanomedicine. Front. Bioeng.Biotechnol. *5*, 1–8.

Gong, Y., Adhikari, P., Liu, Q., Wang, T., Gong, M., Chan, W.L., Ching, W.Y., and Wu, J. (2017). Designing the interface of carbon nanotube/ biomaterials for high-performance ultra-broadband photodetection. ACS Appl. Mater. Interfaces *9*, 11016–11024.

Gorman, G., Chinnery, P., DiMauro, S., et al. (2016). Mitochondrial diseases. Nat. Rev. Dis. Primers *2*, https://doi.org/10.1038/nrdp.2016.80.

Gryszel, M., Rybakiewicz, R., and Głowacki, E.D. (2019). Water-soluble organicdyes as molecular photocatalysts for H 2 O 2 evolution. Adv. Sustain. Syst. *3*, 1900027.

Guo, L., Liu, W., Niu, G., Zhang, P., Zheng, X., Jia, Q., Zhang, H., Ge, J., and Wang, P. (2017). Polymer nanoparticles with high photothermal conversion efficiency as robust photoacoustic and thermal theranostics. J. Mater. Chem. B *5*, 2832–2839.

Huang, Y., Ren, J., and Qu, X. (2019). Nanozymes: classification, catalytic mechanisms, activity regulation, and applications. Chem.Rev. *119*, 4357–4412.

Jiang, Y., and Pu, K. (2018). Multimodal biophotonics of semiconducting polymer nanoparticles. Acc. Chem. Res. *51*, 1840–1849.

Jiang, Y., and Tian, B. (2018). Inorganic semiconductor biointerfaces. Nat. Rev. Mater. *3*, 473–490.

Jiang, Y., Li, X., Liu, B., Yi, J., Fang, Y., Shi, F., Gao, X., Sudzilovsky, E., Parameswaran, R., Koehler, K., et al. (2018). Rational design of silicon structures for optically controlled multiscalebiointerfaces. Nat. Biomed. Eng. *2*, 508–521.

Kang, H., Zhang, K., Pan, Q., Lin, S., Wong, D.S.H., Li, J., Lee, W.Y.W., Yang, B., Han, F., Li, G., et al. (2018). Remote control of intracellular calcium using upconversionnanotransducers regulates stem cell differentiation in vivo. Adv. Funct. Mater. *28*, 1–12.

Krumova, K., and Cosa, G. (2016). Chapter I: overview of reactive oxygen species. In Singlet Oxygen: Applications in Biosciences and Nanosciences, *1*Singlet Oxygen: Applications in Biosciences and Nanosciences, p. 21.

Li, J., and Pu, K. (2019). Development of organic semiconducting materials for deep-tissue optical imaging, phototherapy and photoactivation. Chem. Soc. Rev. *48*, 38–71.

Li, J., Duan, H., and Pu, K. (2019). Nanotransducers for near-infrared photoregulation in biomedicine. Adv. Mater. *31*, e1901607.

Lin, T.E., Rapino, S., Girault, H.H., and Lesch, A. (2018). Electrochemical imaging of cells and tissues. Chem. Sci. *9*, 4546–4554.

De Lonlay, P., Valnot, I., Barrientos, A., Gorbatyuk, M., Tzagoloff, A., Taanman, J.W., Benayoun, E., Chrétien, D., Kadhom, N., Lombès, A., et al. (2001). A mutant mitochondrial respiratory chain assembly protein causes complex III deficiency in patients with tubulopathy, encephalopathy and liver failure. Nat. Genet. *29*, 57–60.

Liu, D., Ma, L., An, Y., Li, Y., Liu, Y., Wang, L., Guo, J., Wang, J., and Zhou, J. (2016). Thermoresponsivenanogel-encapsulated PEDOT and HSP70 inhibitor for improving the depth of the photothermal therapeutic effect. Adv. Funct. Mater. *26*, 4749–4759.

López-Bernabeu, S., Huerta, F., Morallón, E., and Montilla, F. (2017). Direct electron transfer to cytochrome c induced by a conducting polymer. J. Phys. Chem. C *121*, 15870–15879.

Lyu, Y., Xie, C., Chechetka, S.A., Miyako, E., and Pu, K. (2016). Semiconducting polymer nanobioconjugates for targeted photothermal activation of neurons. J. Am. Chem. Soc. *138*, 9049–9052.

Lyu, Y., Tian, J., Li, J., Chen, P., and Pu, K. (2018). Semiconducting polymer nanobiocatalysts for photoactivation of intracellular redox reactions. Angew. Chem.Int. Ed. *57*, 13484–13488.

Lyu, Y., He, S., Li, J., Jiang, Y., Sun, H., Miao, Y., and Pu, K. (2019). A photolabile semiconducting polymernanotransducer for near-infrared regulation of CRISPR/Cas9 geneediting. Angew. Chem. Int. Ed. *58*, 18197–18201.

Malferrari, M., Becconi, M., and Rapino, S. (2019a). Electrochemical monitoring of reactive oxygen/nitrogen species and redox balance in living cells. Anal.Bioanal. Chem. *411*, 4365–4374.

Malferrari, M., Ghelli, A., Roggiani, F., Valenti, G., Paolucci, F., Rugolo, M., and Rapino, S. (2019b). Reactive oxygen species produced by mutated mitochondrial respiratory chains of entire cells monitored using modified microelectrodes. ChemElectroChem *6*, 627–633.

Maya-Vetencourt, J.F., Ghezzi, D., Antognazza, M.R., Colombo, E., Mete, M., Feyen, P., Desii, A., Buschiazzo, A., Di Paolo, M., Di Marco, S., et al. (2017). A fully organic retinal prosthesis restores vision in a rat model of degenerative blindness. Nat. Mater. *16*, 681–689.

Moros, M., Lewinska, A., Onorato, G., Antognazza, M.R., Di Maria, F., Blasio, M., Lanzani, G., Tino, A., Wnuk, M., and Tortiglione, C. (2018). Light-triggered modulation of cell antioxidant defense by polymer semiconducting nanoparticles in a model organism. MRS Commun. *8*, 918–925.

Mosconi, E., Salvatori, P., Saba, M.I., Mattoni, A., Bellani, S., Bruni, F., Santiago Gonzalez, B., Antognazza, M.R., Brovelli, S., Lanzani, G., et al. (2016). Surfacepolarization drives photoinduced charge separation at the P3HT/water interface. ACS EnergyLett. *1*, 454–463.

Ohara, A., and Sayuri, M. (2012). Oxygen radicals and related species in principles of free radicalbiomedicine, principles of free radical biomedicine, I. http://site.ebrary.com/id/10686370.

Ow, Y.L.P., Green, D.R., Hao, Z., and Mak, T.W. (2008). Cytochrome c: functions beyond respiration. Nat. Rev. Mol. Cell Biol. *9*, 532–542.

Park, J.H., Lee, S.H., Cha, G.S., Choi, D.S., Nam, D.H., Lee, J.H., Lee, J.K., Yun, C.H., Jeong, K.J., and Park, C.B. (2015). Cofactor-free light-driven whole-cell cytochrome P450 catalysis. Angew. Chem.Int. Ed. *54*, 969–973.

Rapino, S., Treossi, E., Palermo, V., Marcaccio, M., Paolucci, F., and Zerbetto, F. (2014). Playing peekaboo with graphene oxide: a scanning electrochemical microscopy investigation. Chem. Commun.(Camb.) *50*, 13117–13120.

Rapino, S., Marcu, R., Bigi, A., Soldà, A., Marcaccio, M., Paolucci, F., Pelicci, P.G., and Giorgio, M. (2015). Scanning electro-chemical microscopy reveals cancer cell redox state. Electrochim.Acta *179*, 65–73.

Rojas, H.C., Bellani, S., Fumagalli, F., Tullii, G., Leonardi, S., Mayer, M.T., Schreier, M., Grätzel, M., Lanzani, G., Di Fonzo, F., and Antognazza, M.R. (2016). Polymer-based photocathodes with a solution-processable cuprous iodide anode layer and a polyethyleneimine protective coating. Energy Environ. Sci. *9*, 3710–3723.

Soldà, A., Valenti, G., Marcaccio, M., Giorgio, M., Pelicci, P.G., Paolucci, F., and Rapino, S. (2017). Glucose and lactate miniaturized biosensors for secm-based high-spatial resolution analysis: a comparative study. ACS Sensors *2*, 1310–1318.

Song, N.J., Chang, S.H., Li, D.Y., Villanueva, C.J., and Park, K.W. (2017). Induction of thermogenic adipocytes: molecular targets and thermogenic small molecules. Exp. Mol. Med. *49*, https://doi.org/10.1038/emm.2017.70.

Tian, B., and Lieber, C.M. (2013). Synthetic nanoelectronic probes for biological cells and tissues. Annu. Rev. Anal. Chem. *6*, 31–51.

Tian, B., Xu, S., Rogers, J.A., Cestellos-Blanco, S., Yang, P., Carvalho-de-Souza, J.L., Bezanilla, F., Liu, J., Bao, Z., Hjort, M., et al. (2018). Roadmap on semiconductor – cell biointerfaces. Phys. Biol. *15*, https://doi.org/10.1088/1478-3975/aa9f34.

Tortiglione, C., Antognazza, M.R., Tino, A., Bossio, C., Marchesano, V., Bauduin, A., Zangoli, M., Morata, S.V., and Lanzani, G. (2017). Semiconducting polymers are light nanotransducers in eyeless animals. Sci. Adv. *3*, https://doi.org/10.1126/sciadv.1601699.

Tullii, G., Desii, A., Bossio, C., Bellani, S., Colombo, M., Martino, N., Antognazza, M.R., and Lanzani, G. (2017). Bimodal functioning of a mesoporous , light sensitive polymer/electrolyte interface. Org. Electron. *46*, 88–98.

Wang, Y.P., and Lei, Q.Y. (2018). Metabolite sensing and signaling in cell metabolism. Signal.Transduct. TargetTher. *3*, 1–9.

Wang, Y., Li, S., Zhang, P., Bai, H., Feng, L., Lv, F., Liu, L., and Wang, S. (2018). Photothermal-responsive conjugated polymer nanoparticles for remote control of gene expression in living cells. Adv. Mater. *30*, 1–5.

Wittstock, G., Burchardt, M., Pust, S.E., Shen, Y., and Zhao, C. (2007). Scanning electrochemical microscopy for direct imaging of reaction rates. Angew. Chem. Int. Ed. *46*, 1584–1617.

Yeagle, P.L. (2011). Membrane proteins. The Structure of Biological Membranes, Third Edition. https://doi.org/10.1016/B978-0-12-800047-2.00010-3.

Zhu, J., and Thompson, C.B. (2019). Metabolic regulation of cell growth and proliferation. Nat. Rev. Mol. CellBiol. *20*, 436–450.

iScience, Volume *23*

Supplemental Information

Light-Triggered Electron Transfer between a Conjugated Polymer and Cytochrome C for Optical Modulation of Redox Signaling

Ilaria Abdel Aziz, Marco Malferrari, Francesco Roggiani, Gabriele Tullii, Stefania Rapino, and Maria Rosa Antognazza

Supporting Figures

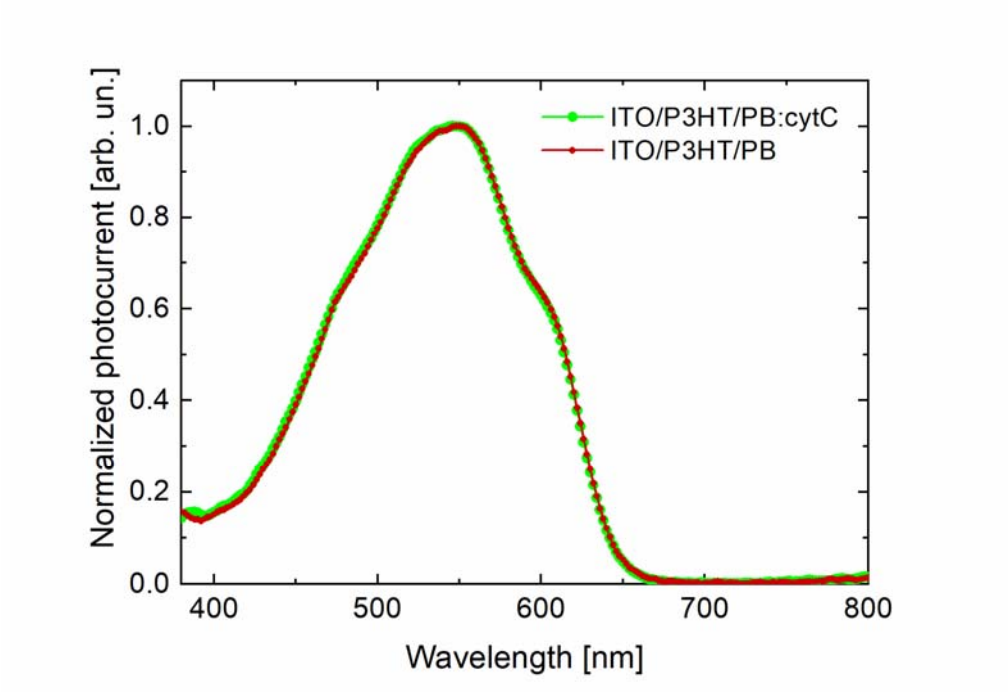

Figure S1. **Photocurrent action spectrum of ITO/P3HT/PB and ITO/P3HT/PB:CytC** (Related to Figure 1). The photocurrent action spectrum of ITO/P3HT in phosphate buffer (red dotted line) and in CytC-enriched PB solution (green dotted line) was recorded in a two-electrodes electrochemical cell coupled with a lamp, a monochromator and a photodiode. The signal was acquired by means of a lock in amplification system.

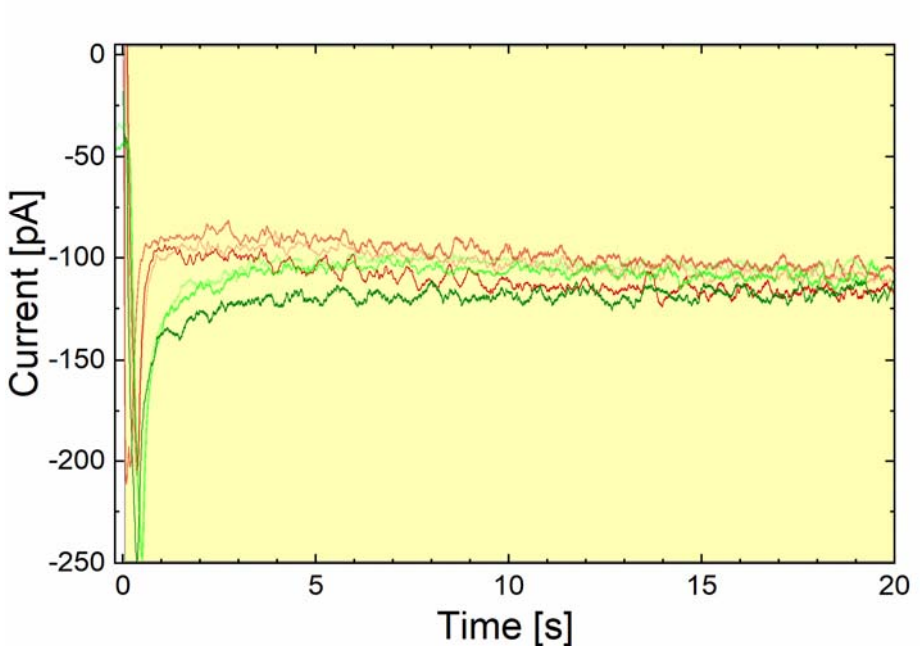

Figure S2. Chronoamperometry recording hydrogen peroxide production upon illumination (Related to Figure 1). Time course of hydrogen peroxide production upon polymer photoexcitation, in 4 mM phosphate buffer. Red, light red and orange have been recorded in absence of CytC; Dark green, light green and green traces are recorded in presence of 10 μM CytC. See Transparent methods for details on trace treatment.

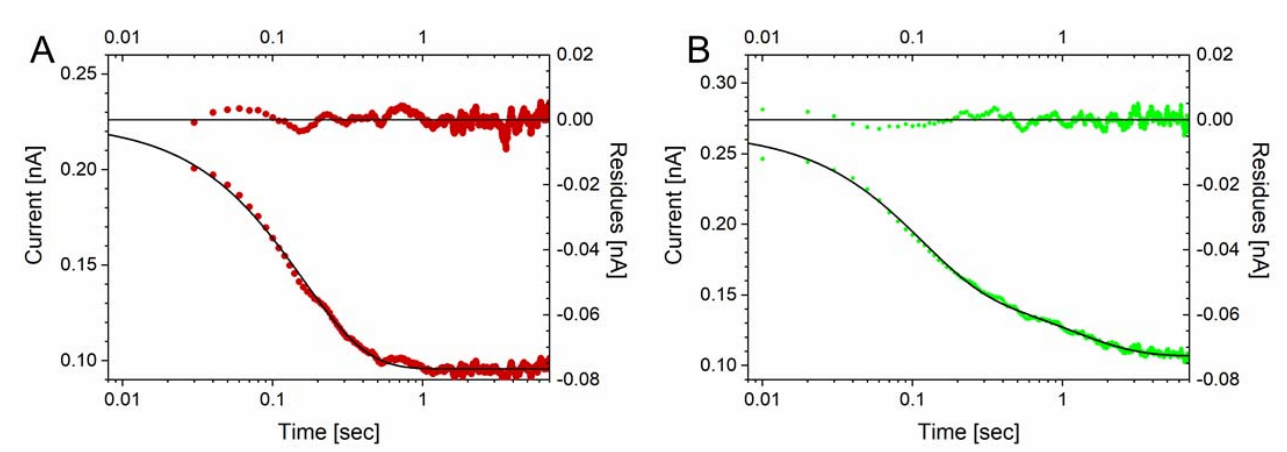

Figure S3. Fitting of chronoamperometry after the light onset (Related to Figure 1). Exponential fitting of the current observed in the time corse experiments, in absence (panel A) and in presence (panel B) of CytC. In both panels, the lower part report the experimental data as dotted lines and the exponential fitting curve as a black solid line, while in the upper part the residues are presented. The left axis refers to the experimental data, while the right axis to residues. In the ITO/P3HT/PB system a single exponential decay was used; for the system ITO/P3HT/PB:CytC a two-exponential fitting was necessary, based on the residues analysis.

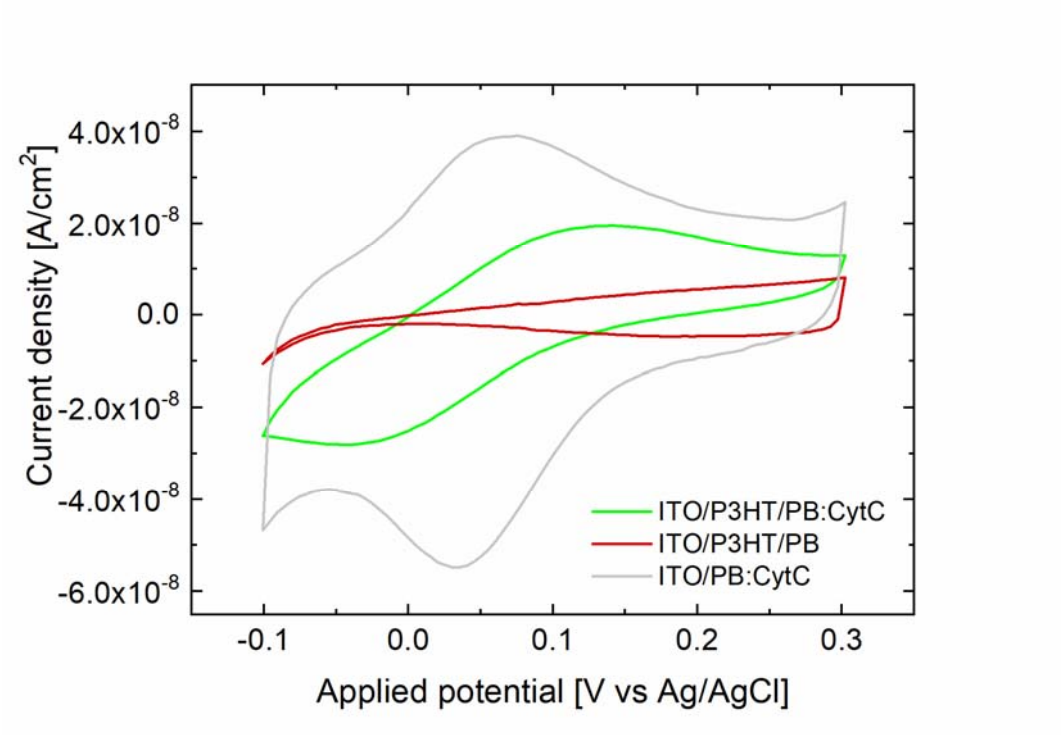

Figure S4. Cyclic Voltammetry of ITO/P3HT device in contact with CytC (Related to Figure 1). Cyclic voltammetry of ITO/P3HT working electrode in bare phosphate buffer (PB, red line) and in CytC-enriched PB (PB:CytC, 1 μM solution, green solid line). ITO working electrode in CytC-enriched PB (PB:CytC, 1 μM solution, grey solid line) is also shown for reference.

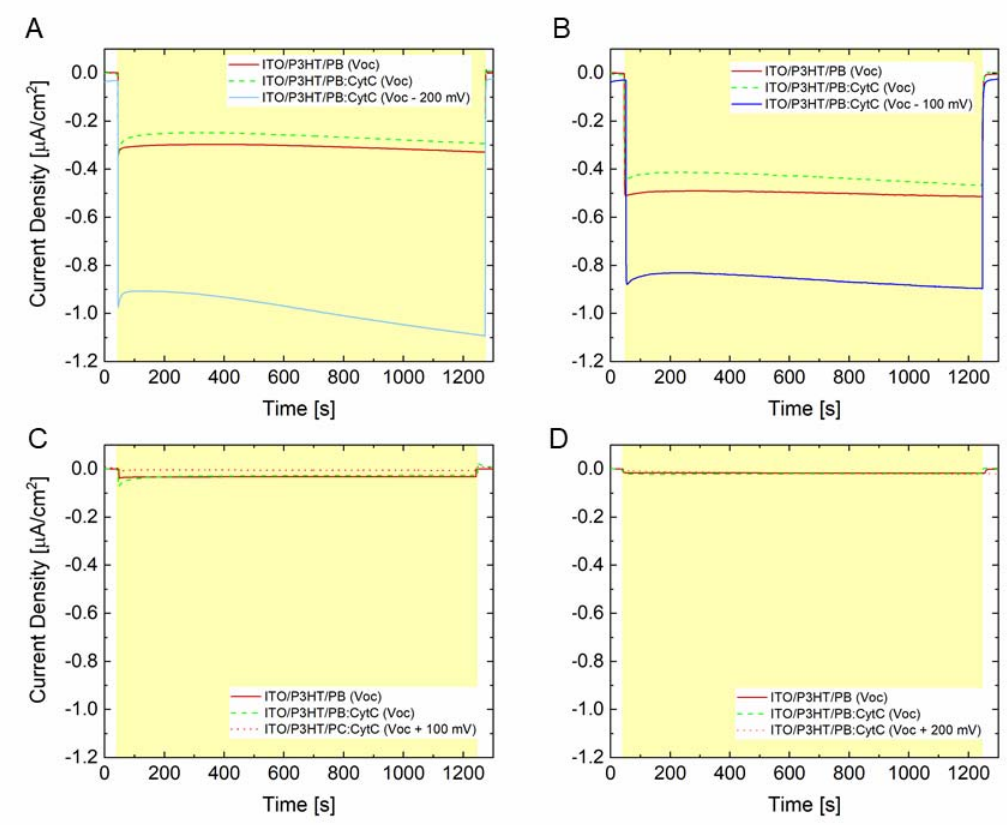

Figure S5. Photocatalytic activity of ITO/P3HT device in PB (Related to Figure 3). Chronoamperometry measurements upon externally applied positive and negative bias recorded during spectroelectrochemical measurements in a three electrodes electrochemical cell. In all panels, ITO/P3HT/PB photocurrent generated at open circuit potential vs Ag/AgCl in phosphate buffer is reported as a black solid line, ITO/P3HT/PB:CytC 10 μM at V_{OC} is reported as a dashed red line, ITO/P3HT/PB:CytC 10 μM at $V_{OC} \pm V_{app}$ is reported as a solid red line. The panels **A**, **B**, **C**, **D** are related to $V_{OC} - 0.2$ V, $V_{OC} - 0.1$ V, $V_{OC} + 0.1$ V, $V_{OC} + 0.2$ V vs Ag/AgCl, respectively. The yellow shaded area displays the illumination period, lasting for 20 minutes.

According to the photocathodic behaviour of the polymer/buffer interface, the bias negative respect to the V_{OC} value promotes electron transfer processes at the polymer surface, thus increasing the absolute value of the photocurrent density. Conversely, a bias more positive than the V_{OC} value hampers polaron dissociation and free electrons formation at the interface with the electrolyte, thus possibly reducing the overall oxygen reduction reaction efficiency and the photocurrent density absolute value. In this experimental configuration, the addition of CytC to the buffer does not lead to remarkable changes in the photocurrent dynamics.

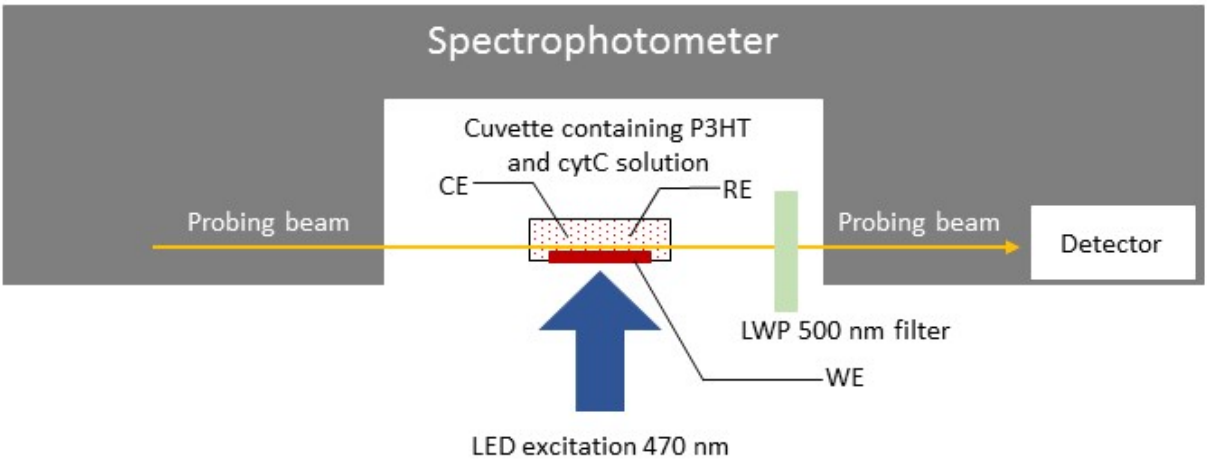

Figure S6. Spectroelectrochemical setup scheme (related to Figure 3 and Figure 4)**.** A cuvette containing ITO/P3HT thin film in contact with a solution containing CytC 10 μM dissolved in phosphate buffer (4 mM, pH 7.4) was positioned through the optical path of the probing beam of the spectrophotometer. The beam was carefully aligned with the cuvette, in order to avoid any interference with the polymer surface (i.e. with the working electrode, WE). The counter and the reference electrodes (CE and RE, respectively) were positioned far from the probing beam. A 470 nm LED was employed to photoexcite the polymer, the excitation optical path being orthogonal to the probing beam. A Long Wave Pass (LWP) filter at 500 nm was positioned at the entrance slit of the detector to avoid the cross talk between probing and excitation beam in the detection phase.

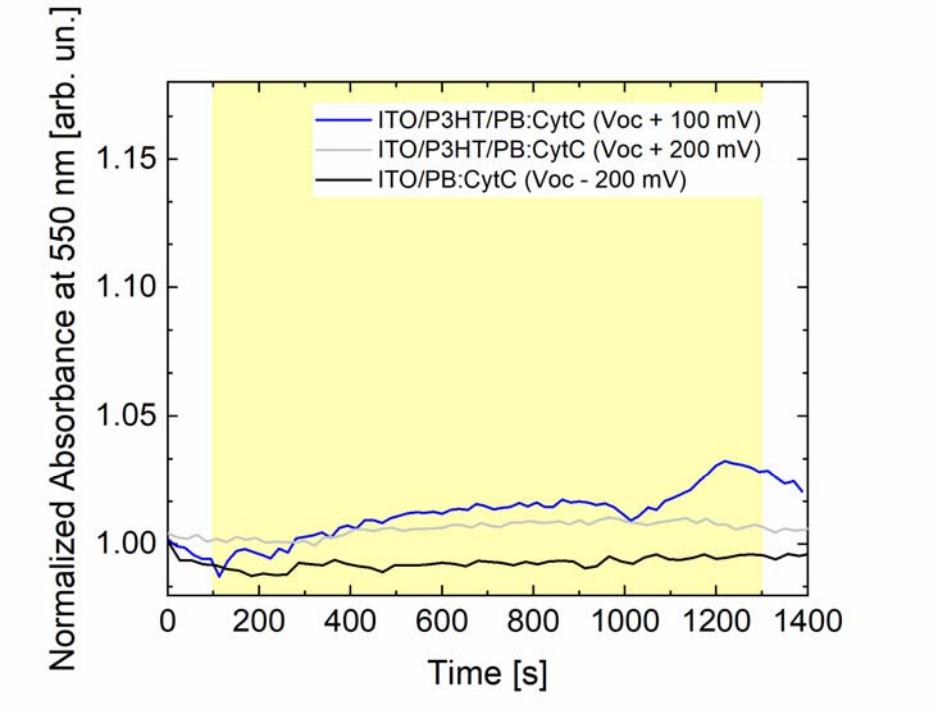

Figure S7. **550 nm peak variation of CytC upon positive biases** (Related to Figure 3). Relative temporal variation of the CytC absorbance peak at 550 nm peak, upon polarization and optical excitation of the ITO/P3HT working electrode, at positive (V_{OC} + 100 mV and V_{OC} + 200 mV, blue and grey lines respectively) and negative bias (V_{OC} – 200 mV). Bare ITO was used as a control substrate. The yellow shaded area shows the illumination period.

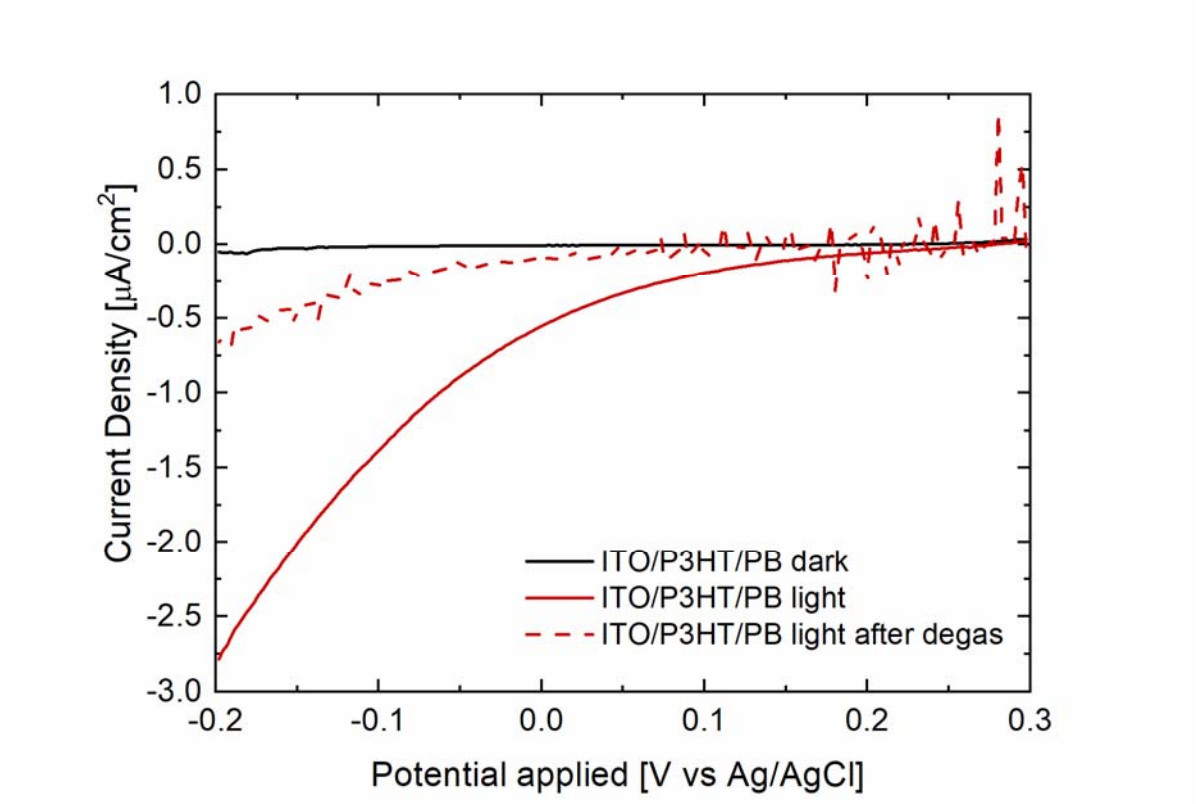

Figure S8. Linear Sweep Voltammetry of ITO/P3HT device upon nitrogen purging (Related to Figure 4). Linear sweep voltammetry (LSV) of ITO/P3HT working electrode recorded in a three electrodes electrochemical cell. LSVs were recorded in phosphate buffer in dark condition (black solid line), upon optical excitation of the ITO/P3HT electrode (red solid line) and upon removal of oxygen from the solution (red dashed line).

Transparent Methods

1 Sample preparation.

Poly-3-Hexyl-Thiophene (P3HT) polymer (15000-45000 MW, Sigma Aldrich) was dissolved in Chlorobenzene (Sigma Aldrich) up to a final concentration of 20 mg/mL. The solution was stirred at 65 °C for 6 hours. Indium-Tin-Oxide (ITO)/glass substrates (XynYan Technology, 15 nm thickness, sheet resistance 15 ohm/sq) were subsequently sonicated in water, acetone, isopropanol (10 minutes each). P3HT solution was spin coated (1500 rpm for 1 minute) on the ITO slabs, obtaining a final thickness of 130 nm and an optical density of 0.6 (at the main absorption peak).

Electrochemical measurements.

Chronoamperometry (CA), cyclic voltammetry (CV) and linear sweep voltammetry (LSV) measurements were carried out with a potentiostat (PGSTAT 302N, AutoLab), in a two-compartments, three electrodes photoelectrochemical cell. The counter and the reference electrodes (platinum wire and saturated KCl Ag/AgCl electrode, respectively) were separated from the working electrode (ITO/P3HT electrode) by a saline bridge. Both CAs and CVs were carried out in Phosphate Buffer (PB), pH = 7.4, 4 mM concentration. CytC from equine heart (Sigma Aldrich) was diluted in phosphate buffer (PB) up to a final concentration of 10 μM. The CA measurements were carried out both in dark and upon polymer photoexcitation. For optical excitation a continuous light source (Thorlabs LED M470L3-C5, 470 nm central emission wavelength) was employed, with a power density of 2.7 mW/mm^2. Light was impinging on the ITO side of the working electrode. CA measurements were carried out first at the open circuit potential (V_{oc}), in absence of external bias, and then by applying a potential difference in the range [V_{oc} - 200 mV, V_{oc} + 200 mV], with 100 mV steps. LSV were acquired in similar conditions, at 5 mV/s scan rate and upon external bias in the range [-200 mV, +300 mV]. CA, CVs and LSVs were also carried out in controlled oxygen concentration, by fluxing nitrogen until the dissolved oxygen concentration was reduced by 80% (evaluated at – 200 mV). Data were recorded using NOVA 1.11 software and analysed by OriginPro 8.5.

Spectro-electrochemistry.

Spectro-electrochemical characterization was carried out by combining potentiostat recordings with optical absorbance spectra measurements (Perkin-Elmer Lambda 1050). Upon photoexcitation of the ITO/P3HT

working electrode, both CytC absorption spectrum and CA measurements were simultaneously monitored, either at the equilibrium potential or upon external bias. In this measurement, a single compartment cell was employed. CytC absorption spectrum was probed in the range 520 nm - 560 nm, 2 nm steps. The ITO/P3HT working electrode was optically excited as previously described. P3HT optical excitation and spectrophotometer beam were in orthogonal configuration (see Figure S5 for the configuration sketch). Any interference between the spectrophotometer beam and the electrodes was carefully avoided. The cell was black-shielded and a high-pass filter (500 nm cut frequency, Thorlabs) was employed at the entrance of the detector. The absorbance variations have been calculated as the difference between the CytC absorbance before and after the illumination protocol, normalized to the absorbance before the stimulus ($\Delta\alpha = (\alpha_{post} - \alpha_{pre})/ \alpha_{pre}$). Spectroelectrochemical measurements were carried out also upon controlled oxygen atmosphere, by fluxing nitrogen until the dissolved oxygen concentration was reduced by 80%. Electrochemical data were recorded with NOVA 1.11, optical data with UV-VIS WinLab Perkin Elmer software, and then merged together with OriginPro 8.5.

Photocurrent action spectrum.

Photocurrent action spectrum was recorded by employing a single compartment, two electrodes electrochemical cell, in which the ITO/P3HT slab acted as the working electrode and a platinum wire was used as the counter electrode. A tungsten light source, filtered by a double grating monochromator and focused on the sample by a spherical mirror, was used for polymer photoexcitation. Photocurrent spectrum was detected by a lock-in technique, at a modulation frequency of 570 Hz. System response (light source emission spectrum, gratings responsivity, optical components) was measured by using a calibrated Si photodiode and was taken into account to properly normalize the spectra. Data were analysed with OriginPro 8.5 software.

Scanning electrochemical microscopy.

Scanning electrochemical microscopy (SECM) studies were carried out both on ITO/P3HT and ITO electrodes. Substrates were placed at the bottom of a Petri dish using Gel-Film (WF-35-X8-A, Gel-Pak). 4 mM phosphate-buffer was employed, with or without 10 μM CytC. The polymer was photostimulated through a mercury lamp of a Nikon Eclipse Ti inverted microscope, filtered with a Nikon Texas Red HYQ cubic filter (excitation wavelength range, 532-587 nm, emission wavelength range, 608-683 nm). The power density of

the photoexcitation source, measured at 550 nm with an optometer at its focal plane, is 70 mW/mm^2. All SECM measurements were carried out with a CHI910B SECM bipotentiostat from CH Instruments Inc. (Austin, Texas), employing an Ag/AgCl (KCl 3 M) as reference electrode and a platinum wire as counter electrode. Platinum microelectrodes (CHI Pt 10 μm diameter, RG 10) were employed as working electrodes; ultramicroelectrodes were modified with nanoporous black platinum by electrodeposition, as previously described, in order to increase the sensitivity towards hydrogen peroxide. The approach curves were carried out by applying a bias of 0.6 V or -0.7 V (for the positioning of the ultramicroelectrode at 25 μm from the substrate) vs Ag/AgCl (KCl 3 M) at the microelectrode. The current signals reported in the SECM approach curves were normalized to the i_{inf} value, namely the bulk current estimated applying 0.6 V vs Ag/AgCl (KCl 3 M) at a distance higher or equal to 350 μm. Scan lines were carried out in constant height mode. Fitting of decay kinetics of Figure 1D were performed by least-squares minimization routines based on grid search algorithms, using a *in house* developed software. Figure presentation: an offset at 25 s after switching on the illumination has been applied to time coarse of hydrogen peroxide production (Figure 1C), to compare kinetics in presence or absence of CytC, thus eliminating contributions due to the fouling of the black platinum microelectrode.